Analysis and Optimization of Passive Knee Prosthetic Design Parameters over Varying Cadences

by

Krithika Swaminathan

Submitted to the
Department of Mechanical Engineering
in Partial Fulfillment of the Requirements for the Degree of

Bachelor of Science in Mechanical Engineering

at the

Massachusetts Institute of Technology

June 2017

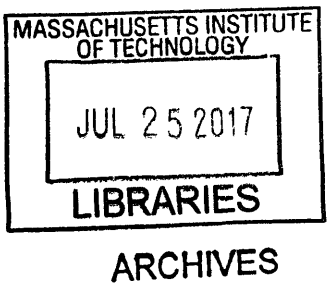

Signature of Author: Signature redacted
Department of Mechanical Engineering
May 18, 2017

Certified by: Signature redacted
Amos Winter
Assistant Professor of Mechanical Engineering
Thesis Supervisor

Accepted by: Signature redacted
Rohit Karnik
Professor of Mechanical Engineering
Undergraduate Officer

Analysis and Optimization of Passive Knee Prosthetic Design Parameters over Varying Cadences

by

Krithika Swaminathan

Submitted to the Department of Mechanical Engineering
on May 1, 2017 in Partial Fulfillment of the
Requirements for the Degree of

Bachelor of Science in Mechanical Engineering

Abstract

The need for effective prostheses is prevalent worldwide, and is especially dire in developing countries and low-resource settings. The MIT GEAR Lab is addressing this gap through the ATKnee, a low-cost, passive prosthetic knee that employs the use of spring and damper components to replicate the knee torque of the able-bodied human knee. In this study, we build upon prior work to optimize the components used in the ATKnee by accounting for results from field-testing. We first develop an inverse dynamics model to confirm understanding of previous work. We then use a genetic optimization algorithm to optimize parameters across different walking speeds and various spring-damper configurations. The best fit, as measured by the highest R^2 value, is obtained when a viscous damper is active during the first dissipative phase (b_{11}^*), a friction damper is active during the second dissipative phase (b_{20}^*), and an additional friction damper is active throughout both phases (b_0^*). We make the suggestion that $b_0^* = 0.084, b_{11}^* = 0.008, b_{20}^* = 0.183$, gives the most optimal passive system knee torque with the engagement and disengagement timings $t_{eng1} = 51.3\%, t_{dis1} = 64.2\%$ for the first damper, and $t_{eng2} = 86.1\%$, $t_{dis2} = 95.2\%$ for the second damper. We find that the parameters are robust to subject body mass, but show a positive correlation with walking speed. We conclude that while we are able to suggest an optimized parameter set that includes higher order dampers, it will be important to investigate the effects of cadence, as well as to study the joint torques at the hip, which is further from the foot.

Thesis Supervisor: Amos Winter
Title: Assistant Professor of Mechanical Engineering

Acknowledgments

I would like to thank the following groups and individuals who have been invaluable for the production of this thesis:

- The MIT Biomechatronics group for making their gait study database publicly available, as it formed the base of the work presented here
- The late Professor David A. Winter for his open source database and textbook on biomechanics, which were used to form an understanding of the physical model of walking
- This work builds heavily off of the thesis of Yashraj Narang, and I thank him for his advice as well
- The GEAR Lab for providing me with the resources to complete this research project, including access to their knee prototype design
- Professor Luiz Faria (MIT, Department of Mathematics) for his guidance through the early stages of this project
- Murthy Arelekatti for his guidance and support throughout this thesis project. His insights and mentorship have made this process an incredibly valuable learning experience.

Finally, I would like to thank MIT for giving me the best four years of my life thus far.

Table of Contents

List of Figures

List of Tables

1. Introduction

The World Health Organization (WHO) estimates that there are about 30 million people worldwide who are in need of prosthetic and orthotic devices [1]. Of these individuals, approximately 3 to 4 million are based in the developing world. The same study found that nearly 90% of all disabled persons in developing nations are isolated from major healthcare advances, without access to quality treatment. In the United States, and other developed nations, it is not uncommon to spend upwards of tens of thousands of dollars on a prosthetic device. These prices are exorbitant even by the standards of developed countries, meaning that the majority of amputees globally are left with little to no means of getting around, and that those who are socioeconomically disadvantaged are further marginalized. Mobility is a human right, and thus the disparity between healthcare economies is a detriment to the progress of humankind.

Amputees who are unable to regain normal gait patterns have been found to experience a lower standard of living [2]. With many careers in developing countries dependent on labor-intensive work, individuals without fully-functioning limbs often remain unemployed. Lack of employment then leads to poverty, further widening the gap between amputees and existing prosthetic solutions. Current attempts to cater to low-cost environments fail for a number of reasons. The conventional approach of simplifying technology available in the high-cost market results in poor quality products. These products are ignorant of the different functional requirements needed when designing for developing world markets, and thus, are unable to withstand the weather and environmental conditions in their target locations. Alternative approaches fail to reproduce normative gait patterns, worsening existing social stigma. Another ramification of abnormal gait is the increased toll on other muscles in the body such as the hip and back muscles, which can cause additional complications [3], [20]. Therefore, a successful solution must be affordable, discreet, comfortable, and enable normal gait.

In order to address the issues of cost and performance, we propose the concept of a passive prosthetic device, which uses a system of mechanical elements to replicate able-bodied gait patterns. The benefits of eliminating electronic and active components are two-fold:

1. Amputees are not limited by access to power sources
2. Spare parts for repairs can easily be salvaged from machinery that are more readily available, such as bicycles and water pumps

We choose to focus on the knee in particular as it is a critical joint in determining gait characteristics [4], specifically for above-the-knee amputees. Furthermore, improper knee function has been found to be one of the costliest determinants of pathological gait [5]. The current gold standard for a passive knee joint is the Stanford-Jaipur Knee (Jaipur, India), which uses a four-bar linkage to model the knee. The knee achieves affordability, with a price of 25 USD per unit [6]. Despite its success, the Jaipur knee still fails to address issues such as frequent mechanical failure and low user-satisfaction. We aim to develop a passive prosthetic knee, the ATKnee, priced around 100 USD per unit, which iterates upon the Jaipur-Stanford knee and effectively addresses user needs.

This work focuses specifically on optimizing the parameters of the mechanical elements of the knee by changing the damping coefficient and order. Prior work done to determine the optimal

configuration of springs and dampers found that a first-order torsional spring and zeroth-order dampers used in conjunction with one-way clutches would be the optimal configuration to approximate the knee dynamics data obtained from able-bodied subjects [7]. However, there are a few points for improvement upon this analysis that will be taken up through this study. This thesis will result in a suggestion for the optimal parameters to be used in the next iteration of the ATKnee in order to achieve the best fit and comfort for patient use. Lastly, this study will explore the effects of mass and cadence on primary contributors to knee dynamics to inform future lines of research.

1.1 Definitions

In this section, we will define the quantities and relevant terms that we use throughout the remainder of the paper.

1.1.1 Gait Cycle

The gait cycle refers to the periodic motion of each leg as an individual progresses from heel strike, the time at which the heel makes initial contact with the ground, to the next heel strike. A schematic of this process is depicted in Figure 1. Biomechanical data is often plotted against percentage of the gait cycle to allow for comparison across the motion of different limbs of one individual as well as to for comparison across a number of subjects. Other physiological metrics such as electromyogram (EMG) measurements, heart rate, weight distribution, and metabolic rate, are also typically plotted against the gait cycle. Each step is divided into the stance phase and swing phase. The stance phase refers to the portion of the time during which the foot is in contact with the ground, while the swing phase occurs right after "toe-off" until the following heel strike event. "Toe-off" generally occurs at around 60% of the gait cycle. The stride length is defined as the length of two steps. Cadence is the number of steps taken per unit time, and is a measure of walking speed that eliminates the effects of varying limb lengths. The gait cycle is relatively independent of time and speed[1] , and thus can be an effective basis for designing robust controllers when dealing with lower limb prostheses and rehabilitative robots.

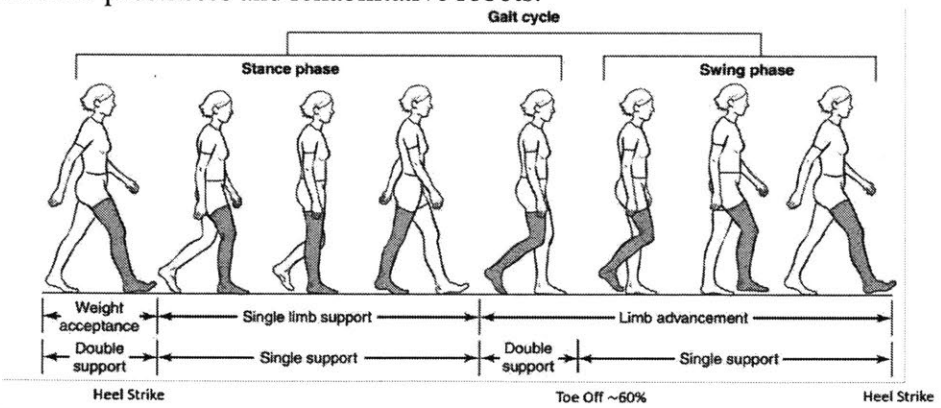

Figure 1 Schematic of the subdivision of the gait cycle into the stance and swing phases, beginning at heel strike and continuing until the following heel strike. The cycle is further subdivided into single and double support phases. Figure adapted from https://s3.amazonaws.com/classconnection/

[1] We will later address the importance of considering variation over different walking speeds. However, the gait cycle is often used as a reliable reference across varying conditions when comparing across people.

1.1.2 General Anatomy

The human body is divided into three planes: the sagittal plane, the coronal plane, and the transverse plane (see Figure 2). The sagittal plane separates the left and right halves, the coronal plane separates the front and back halves, and the transverse plane separates the top and bottom halves of the body. Body segment movements are defined in relation to these planes and other anatomical markers.

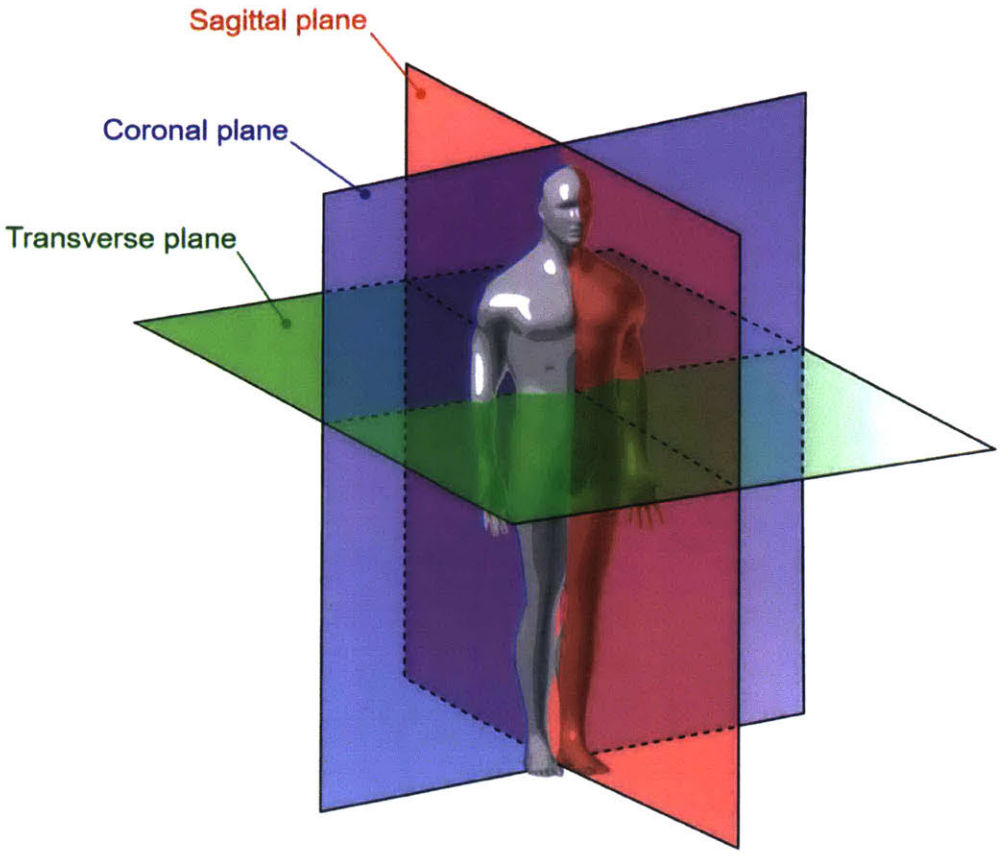

Figure 2 Visualization of the three anatomical body planes. Body segment movements are defined in relation to these planes. Figure adapted from [8]

1.1.3 Knee Biomechanics

Knee angles and torques are commonly used biomechanical data to define gait patterns. We model the knee as a 1 DOF hinge joint, with motion only occurring in the body's sagittal plane [9]. The knee angle is defined as the angle between the thigh and shank segments [10]. The leg is defined as being in flexion when the knee angle is increasing, and in extension when the knee angle is decreasing. In this study, we define flexion as positive and extension as negative as per convention. See Figure 3 for a schematic for the knee angle and the normal knee joint kinematic profile for an able-bodied human through the gait cycle.

This convention is used for ankle and hip angles as well, with flexion movements increasing joint angle and extension movements decreasing joint angle. Thus, correspondingly, positive torques

are those that result in flexion while negative torques lead to extension. In this study, we neglect the movement of the upper body, and these are taken to be the only relevant biomechanical entities.

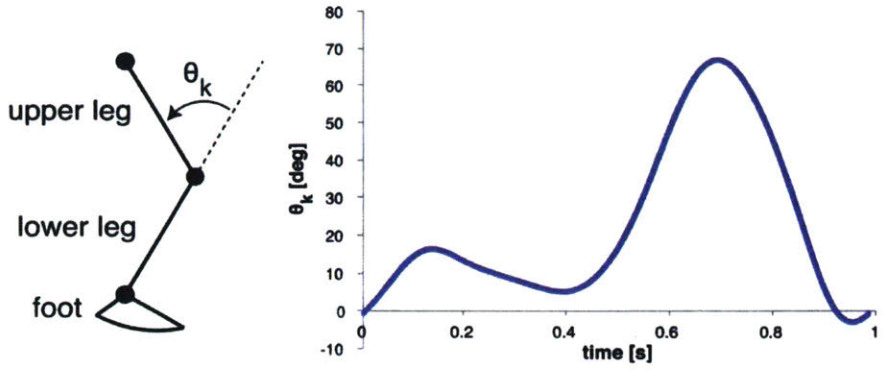

Figure 3 Definition of knee angle (left). Knee angles through the gait cycle in able-bodied gait (right). Figure from [11]

1.2 Prosthetic Knee Design and Control

The current prosthetic knee prototype has three axes of rotation – the knee axis, the early-stance flexion axis, and the locking axis (see Figure 4). The axis of rotation of the knee at any given point is a function of in which phase of the gait cycle the leg is. The relative positions of these axes with respect to the ground reaction force vector throughout the gait cycle determine the torque on the knee joint, and therefore, the motion of the leg. The knee joint itself currently consists of a single first-order torsional spring, two zeroth-order dampers, and a system of clutches to engage and disengage each component at appropriate points during the gait cycle (see Figure 5). The spring is used to store and release energy during heel strike and early stance phase. The two dampers are used to dissipate power during the late stance and swing phases. These components were chosen based on a power analysis done previously that showed that power is purely dissipated during the late stance and swing phases, while it is dissipated and regenerated in the early stance phase [11].

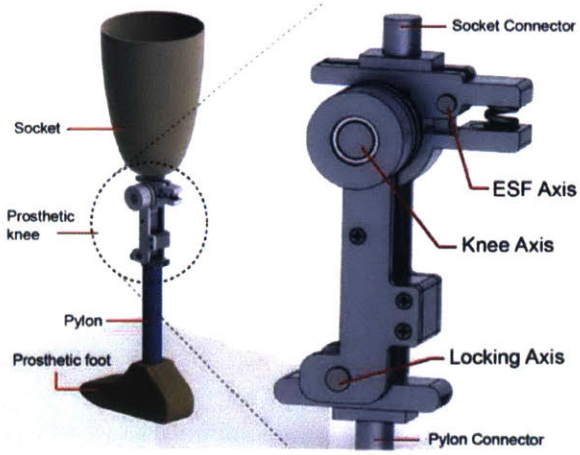

Figure 4 Schematic of the current passive prosthetic knee design. The three axes – the knee axis, the early-stance flexion axis, and the locking axis – are the axes of rotation at different points along the gait cycle. Figure from [12]

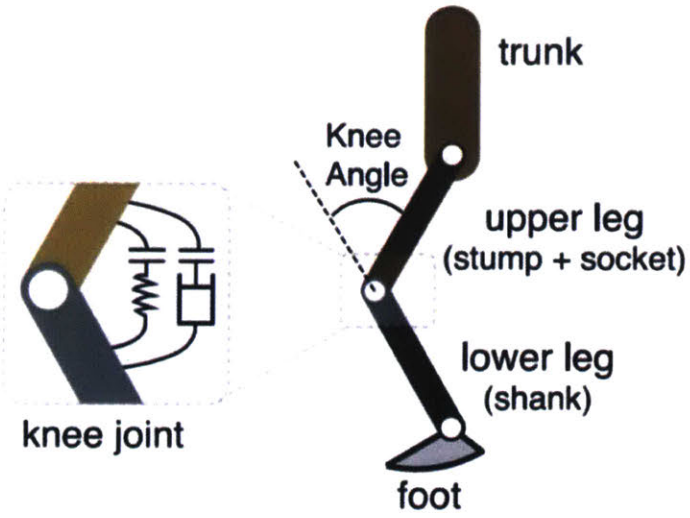

Figure 5 The current prosthetic knee comprises of a first-order spring, two zeroth-order dampers, and a set of one-way clutches to engage and disengage each component at specific points in the gait cycle. Figure from [7]

Prior work has resulted in an optimized spring that is able to replicate the knee torque during early stance reliably [11]. Hence, this study focuses specifically on optimizing the damping mechanism in the knee. The two dampers in the knee work together through differential damping. A force balance on the knee joint yields a relationship between the size of the two dampers as a function of the torques during extension and flexion. Thus, once we determine the necessary torque profile, we can easily find the dimensions of the corresponding differential damping system.

1.3 Caveats in Prior Work

As mentioned earlier, the current parameters for the knee design were determined by Narang in his master's thesis [11]. We wish to improve upon the optimization on a few points through this study.

Narang uses the Winter biomechanics dataset [10] to conduct his analysis. The data includes comprehensive motion capture data from an able-bodied female of mass 56.7kg. The data contains measurements of the linear and angular positions, velocities, and accelerations for two strides as the subject walks across a force plate. However, since there are only two data points for each point in the gait cycle, we are faced with potentially very large errors. Furthermore, as the subject walked at a self-selected speed, we only have data from a speed that is considered reasonable by an able-bodied individual. We know from observation that amputees average lower self-selected walking speeds, and thus, it is important to look at the effects of cadence on the biomechanics. Moreover, the Winter dataset does not contain complete anthropomorphic information for the subject, and as a result, limb segment lengths, and therefore, moment arms, are approximated for the motion. We investigate a number of more recent datasets to work with in this study that are more cohesive and contain data for multiple subjects over varying speeds.

The second point that we address in this study is the performance of the dampers. The current design employs zeroth-order dampers, which are functionally equivalent to friction pads. In practice, this leads to many repercussions associated with the change in friction coefficient as the amputee moves between the static and kinetic regimes. Moreover, abrupt changes in velocity can be dangerous for the user and cause falling. Thus, we focus on the introduction of a first-order

damping component to smoothen the transitions between phases and allow for a more continuous gait.

Finally, we experiment with phase divisions of the gait cycle and timing of engagement and disengagement for each component. Narang divided the gait cycle into three sections based on a power consumption argument. Figure 6 depicts the previously optimized control scheme, with no activity in between phases of engagement. Unlike in the schematic, in the physical model, there is at least one mechanical element that is engaged at any given time. Working with the prototype, we see that it is more practical to segment the cycle based on joint angles and velocities. The optimizations presented here, thus, also optimize the timing of engagement of the dampers.

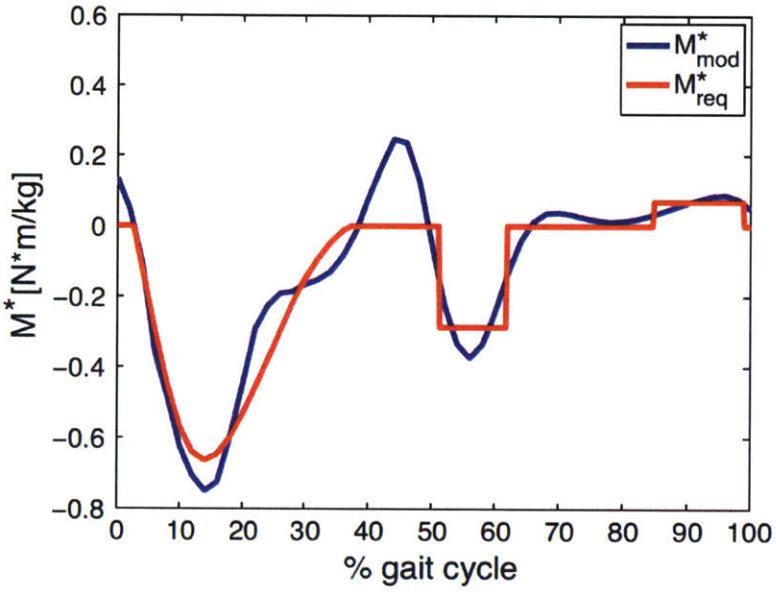

Figure 6 Previously optimized passive system knee torque profile plotted over data. Figure from [11]

2. Methods

In this section, we will explain the methodologies used to model the knee dynamics and to obtain the optimal damping parameters for the passive knee prosthetic. In the scope of this study, we focus on modeling the torque from an able-bodied individual as this allows us to validate the model before expanding to amputee gait parameters. We begin by developing an inverse dynamics model that is able to reproduce the results obtained by Narang [11]. This ensures that the model has an appropriate understanding of the prosthetic design and has the capability to determine optimal parameters for different datasets that contain the necessary input information. We then select a dataset that is most apt for conducting this optimization study. Finally, we define our phase division criteria and run the optimization with various spring-damper configurations. Note that all computations have been done using MATLAB (Mathworks, Natick, MA).

2.1 Inverse Dynamics Model

We assume that the knee is a 1DOF hinge joint, and thus, we can model the leg as a multi-segment link that only moves in one plane. We use a 2-dimensional inverse dynamics approach, capitalizing upon principles of Newtonian mechanics, to calculate the joint moments from the ground reaction force (GRF) and joint angles. We use superposition to isolate the dynamics of one leg by introducing reaction forces and moments where the hip meets the torso. We can further apply this technique to each link of the leg - the foot, the lower leg, and the upper leg. Figure 7 contains the free body diagrams for the foot and shank segments with reaction moments and forces included at the ankle and knee joints.

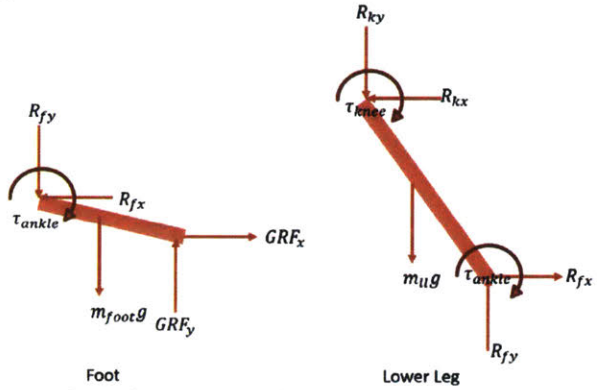

Figure 7 Free body diagram for the foot segment (left) and the shank segment (right). Superposition allows for the independent analysis of each segment

Calculating the reaction forces R_{f_x} and R_{f_y}, and torque τ_{ankle} for the ankle from the respective force and torque balance relations, we have the following system of equations:

$$R_{f_x} = GRF_x - m_f a_{f_x} \tag{2}$$

$$R_{f_y} = GRF_y - m_f a_{f_y} - m_f g \tag{3}$$

$$\tau_{ankle} = I_{ankle} a_{ankle} - m_f g r_{fwt} - GRF_x r_{GRF_x} - GRF_y r_{GRF_y} \tag{4}$$

In equations 2 through 4, GRF refers to the ground reaction force, m refers to the mass of the foot segment, a is the linear acceleration of the foot's center of mass, I_{ankle} is the moment of inertia at the ankle joint, g is the gravitational acceleration, and the r terms are the moment arms for each corresponding force. Similarly, for the knee, we have:

$$R_{k_x} = R_{f_x} - m_{ll} a_{ll_x} \tag{5}$$

$$R_{k_y} = R_{f_y} - m_{ll} a_{ll_y} - m_{ll} g \tag{6}$$

$$\tau_{knee} = I_{knee} a_{knee} - m_{ll} g r_{ll_{wt}} - \tau_{ankle} + R_{f_x} r_{R_{f_x}} + R_{f_y} r_{R_{f_y}} \tag{7}$$

Equations 5 through 7 follow the same notation as equations 2 to 4. The subscript ll refers to the lower leg or shank segment.

In order to confirm that our inverse dynamics model provides a reasonable estimate of the knee torque profile given kinematic and anthropomorphic data, we compare our results with the Winter torque data at the ankle, knee, and hip joints (see Figure 8). We use kinematic and force data from the Winter dataset, and anthropomorphic data cited by Narang [11]. We divide the torques by body mass to obtain a normalized torque that can be compared across individuals. We find that $R^2 = 0.9996$ for the ankle torque, $R^2 = 0.9609$ for the knee torque, and $R^2 = 0.8396$ for the hip torque. Thus, as we move further away from the ground reaction force, the quality of fit reduces. This is an expected trend since uncertainties and errors at the ankle are exacerbated at the knee and hip as a result of being multiplied by moment arms. We note that the model fits the data very well, with an R^2 value greater than 95% for the ankle and knee profiles, and we can use it as the ideal profile to which the passive system is optimized.

2.2 Spring-Damper System

We only model a spring and damper system across the range of knee angles that the leg goes through during one step. Equations 8 and 9 give the contribution to net moment from a spring and from a damper respectively, where θ is the knee angle, and θ_{eq} is the spring's equilibrium position.

$$\tau_{spring} = -\text{sgn}(\theta - \theta_{eq})k_0 - k_1(\theta - \theta_{eq}) - \text{sgn}(\theta - \theta_{eq})k_2(\theta - \theta_{eq})^2 \quad (8)$$

$$\tau_{damper} = -\text{sgn}(\dot{\theta})b_0 - b_1\dot{\theta} - \text{sgn}(\dot{\theta})b_2\dot{\theta}^2 \quad (9)$$

These equations are only applicable for $\theta_{dis} \leq \theta \leq \theta_{eng}$, i.e., while the component is engaged. The contribution to net moment is 0 Nm at all other positions, as we assume that the springs and dampers can be modelled as frictionless. The first, second, and third terms of each equation map to the zeroth, first, and second orders of the components respectively. Thus, the total moment generated by this configuration across the gait cycle is given by Equation 10, with each component generating torque only within its active range.

$$\tau_{passive} = \tau_{spring} + \tau_{damper,1} + \tau_{damper,2} \quad (10)$$

2.3 Dataset Selection

As detailed in section 2.2, we use data from the Winter biomechanics dataset, found in Winter's 4th edition book, as the input for our inverse dynamics method [10]. This dataset also includes the center of pressure coordinates and ground reaction forces, which completes the set of information needed to invoke the inverse dynamics method. Figure 8 presents a schematic of the flow of information to conduct the inverse dynamics.

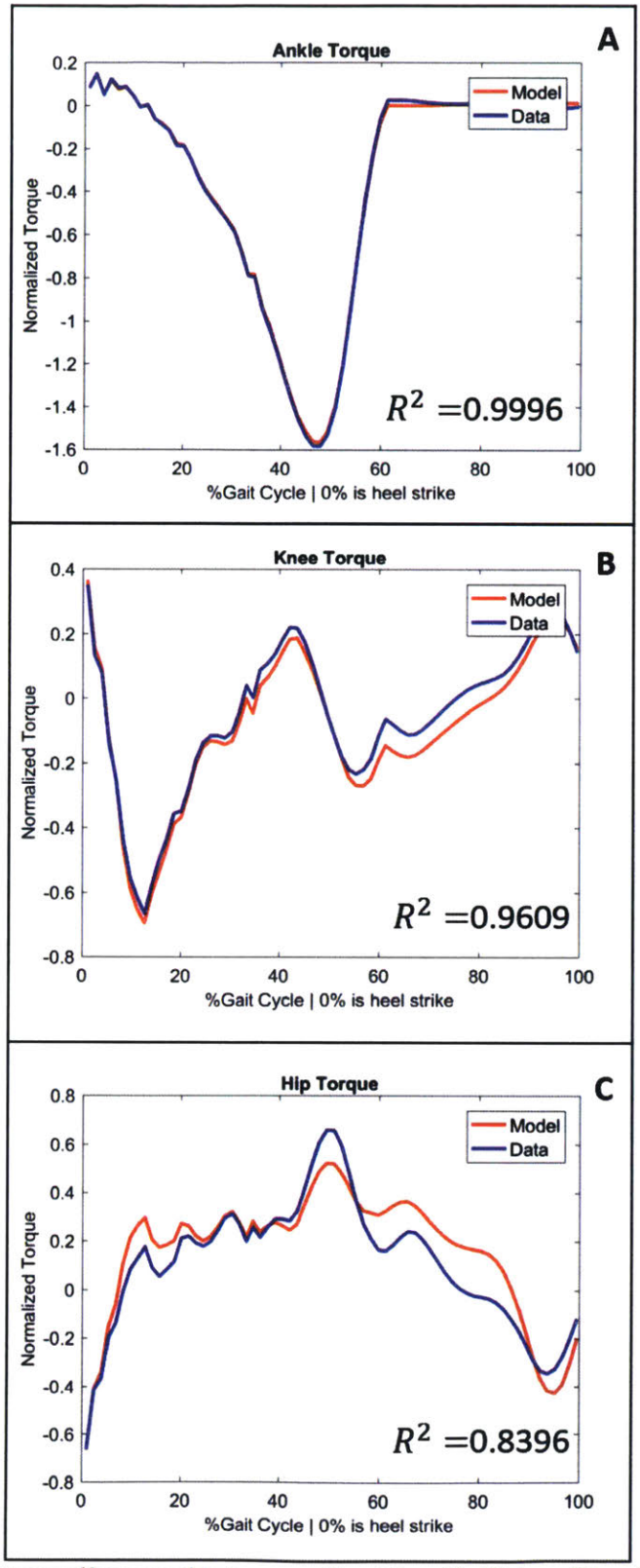

Figure 8 Model torque profiles versus data torque profiles at the ankle (A), knee (B), and hip (C). We see that there is very good fit (R^2 > 0.95) for the ankle and knee torques.

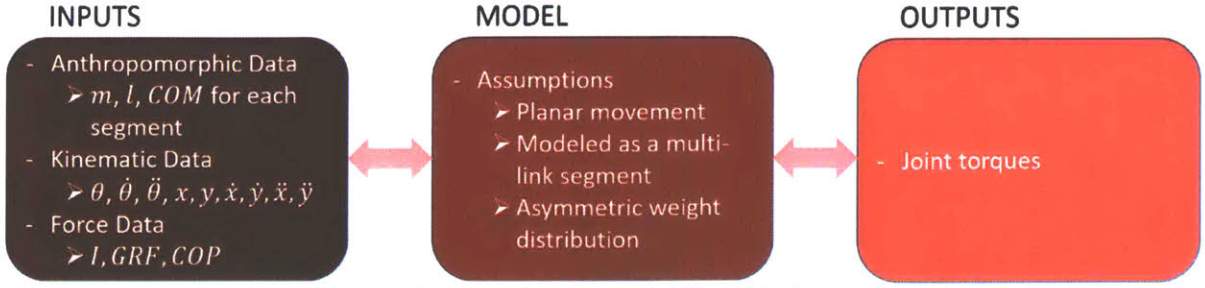

Figure 9 Flow diagram depicting the inverse dynamics methodology and relevant information

We evaluated a number of open-source biomechanics datasets before selecting the dataset published by the MIT Biomechatronics group [13]. Across the Human Motion Dynamics (Germany), OpenSim (Stanford, CA) databases, and CGA Normative Gait database (various), the selected dataset contains the most comprehensive information with kinematic, dynamic, and anthropomorphic data for five able-bodied adult male subjects. The subjects walk at 0.75 m/s, 1.00 m/s, 1.25 m/s, 1.50 m/s, 1.75 m/s, 2.00 m/s, for seven minutes each. Furthermore, the torque profiles at each joint, as calculated by SIMM (Evanston, IL), are also provided, eliminating the need to conduct the inverse dynamics model independently. We verify that the data is reliable for our analysis by plotting the mean knee torque profile of each subject against that of the Winter data over the gait cycle (see Figure 10). We use data from the subjects walking at 1.5 m/s, as this is closest to the self-selected speed of approximately 1.4 m/s in the Winter experiment. The knee torques are normalized by body mass to reduce mass effects. From Figure 10, we see that there is a good fit between the two datasets, and conclude that we can safely use this dataset as we proceed with the study.

2.4 Optimization Criteria

We use the method of mechanical model coefficients to optimize the coefficients in Equations 8 and 9. This method involves defining a cost function and running an optimization algorithm to either minimize or maximize the cost depending on the application. For this study, we define the cost as a measure of the fit between simulated passive knee torques and the ideal profile, the chosen dataset. We calculate the joint moment at each percentage of the gait cycle so that each pair of corresponding points serves as a point of comparison.

From Narang's work, we find that the optimized spring parameters are $k_0 = 0, k_1 = 2.9\frac{N \cdot m}{kg \cdot rad}, k_2 = 0$. Furthermore, these values were found to be robust to different configurations and cadences, and thus, we will consider them as optimized and focus on optimizing the damper configuration. Due to price constraints, we only look at varying zeroth and first order damping. Hence, we are optimizing b_{10}, b_{11}, b_{20}, and b_{21}, as well as $t_{eng1}, t_{eng2}, t_{dis1}, t_{dis2}$, where b_{ij} refers to the coefficient of the j^{th} order term of the i^{th} damper, and the times of engagement/disengagement for each damper are in units of percentage gait cycle.

We use the R^2 value for the passive torque curve fitted to the data as the cost function when varying the different parameters. Note that we choose to only fit the joint torques as this is analogous to imitating the muscular activation that occurs in able-bodied individuals. Furthermore, the joint torques in conjunction with anthropomorphic parameters are sufficient to determine joint angles,

which in turn are used to define symmetric gait. The cost form is uniformly weighted across the segment of the gait cycle with $t_{eng1} < t$ as we want the passive knee to match the able-bodied knee closely across the entirety of the gait cycle. We wish to ignore the polarity of the error, and hence a error-squared cost function, such as R^2, enables us to evaluate fit irrespective of sign.

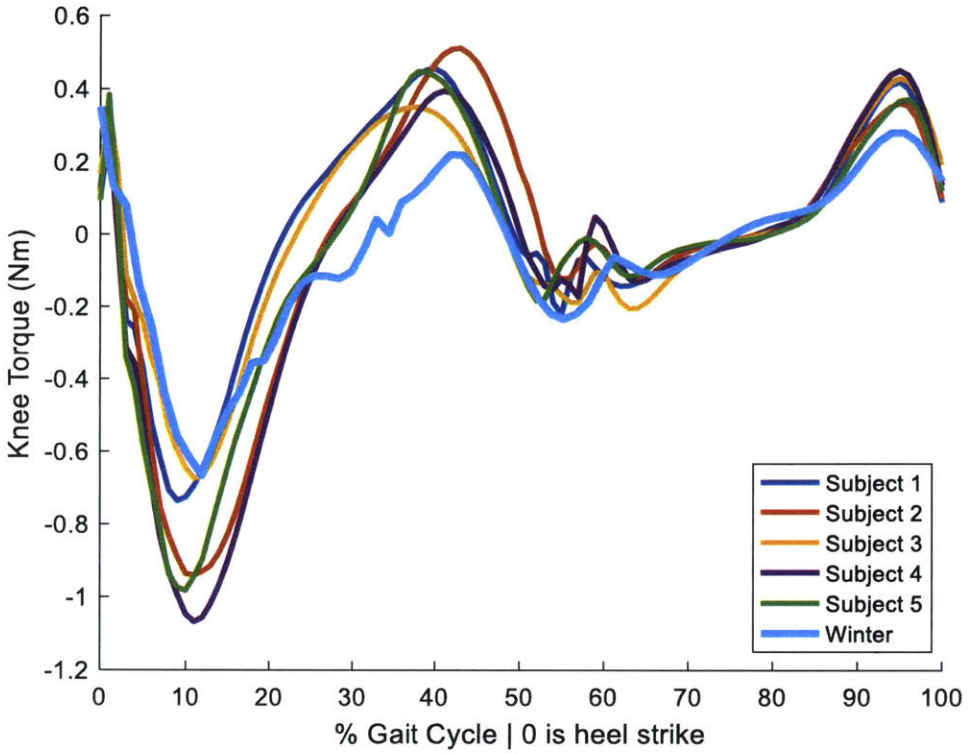

Figure 10 Average knee torque profiles for each subject walking at 1.5 m/s and from the Winter dataset, in which the subject walks at approximately 1.4 m/s. The torque values have been normalized by the subject body mass. The Biomechatronics torque profiles match the Winter torque profiles closely, with the exception of larger extrema values.

We are also optimizing engagement/disengagement timing, on which we place some restrictions to speed the algorithm and to reduce the likelihood of finding multiple local minima. We note that the spring will be responsible for the storage and subsequent regeneration of energy, which is seen as the decrease and increase in knee torque from heel strike to approximately 40% of the gait cycle in Figure 10. We set the first damper to engage at the first zero torque crossing after the spring has disengaged, which typically occurs between 40% and 60% of the gait cycle. From Figure 3, we can also see that there is a peak in knee angle around 80% of the gait cycle. We make the additional requirement that the first damper needs disengage before this peak, and the second damper can only engage past this peak. This constraint is made to ensure that the second damper engages in our optimization algorithm, instead of never engaging. Furthermore, from a design perspective, it is physically possible to construct a damper that engages when the knee velocity is either positive or negative, and disengages in the opposite direction. Finally, we incorporate the physical limitations of engagement and disengagement with the dampers to require each component to be active for at least 3% of the gait cycle as the clutches cannot turn on and off instantaneously. We

define the region in which the first damper is active as phase 2, and the region in which the second damper is active as phase 3.

We use MATLAB's inbuilt genetic algorithm optimization function, ga, to find values that minimize the cost function given its ability to search beyond discontinuities such as those present in our problem here. The function intakes boundary constraints and the cost function, and outputs the optimized parameters for the system.

2.4.1 Optimization Configurations

We run this optimization across four different potential configurations:

- Case 1: Viscous damper in phase 2 and a friction damper in phase 3
- Case 2: Viscous damper in phase 2 and a viscous damper in phase 3
- Case 3: Case 1 with an additional frictional damper through phase 2 to the end
- Case 4: Case 2 with an additional frictional damper through phase 2 to the end

Our updated equation to be fit is given below:

$$\tau_{passive} = \tau_{damp1} + \tau_{damp2} + \tau_{const} \qquad \text{for } t_{eng1} \leq t$$

Where:

$$\tau_{damp1} = -b_{11}\dot{\theta} \qquad \text{for } t_{eng1} \leq t \leq t_{dis1}$$

$$\tau_{damp2} = -\text{sign}(\dot{\theta})b_{20} - b_{21}\dot{\theta} \qquad \text{for } t_{eng2} \leq t \leq t_{dis2}$$

$$\tau_{const} = -\text{sign}(\dot{\theta})b_0 \qquad \text{for } t_{eng1} \leq t$$

Thus, we can rewrite the four cases to be optimized as follows:

- Case 1: $b_0 = 0, b_{21} = 0$
- Case 2: $b_0 = 0, b_{20} = 0$
- Case 3: $b_{21} = 0$
- Case 4: $b_{20} = 0$

The four cases above were optimized with each subject's knee torque data at each speed. We present the results of these optimizations in the following section.

3. Results

This section of the paper discusses the results of our optimization protocol and observed trends in the coefficients across different cadences and masses. We also expound upon interesting points of notice for future work.

3.1 Optimized Parameters

Running the optimization algorithm yields the optimal parameters for each configuration, which are detailed in Tables 1 and 2. Each value is the average over 30 optimized trials (five subjects at six speeds each). The parameters b_0^*, b_{11}^*, b_{20}^*, and b_{21}^* are normalized by dividing by the subject's body mass to remove mass effects. As mentioned earlier, engagement timing of the first damper was set by the torque profile to be the point at which knee torque crosses zero between 40% and 60% of the gait cycle, and thus was not optimized.

Figures 11 through 14 plot the torque profile predicted from the passive system against the torque profiles from the five subjects. We plot these curves as normalized by the body mass in order to provide an accurate comparison across all five participants. Since we have placed a lower boundary on the engagement timing of the first damper at 40%, the curves go from 40% to 100% of the gait cycle, the region we are optimizing. The passive system uses the average position and velocity profiles from the five subjects to calculate the equivalent passive torque of the spring-damper system. R^2 values for each case are listed in Table 1. Again, note that since we are focusing on the damper optimization, R^2 values are only calculated from when the first damper is engaged until the end of the gait cycle.

Case	$b_0\left[\frac{N}{rad}\right]$	$b_0^*\left[\frac{N}{rad \cdot kg}\right]$	$b_{11}\left[\frac{N \cdot s}{rad}\right]$	$b_{11}^*\left[\frac{N \cdot s}{rad \cdot kg}\right]$	$b_{20}\left[\frac{N}{rad}\right]$	$b_{20}^*\left[\frac{N}{rad \cdot kg}\right]$	$b_{21}\left[\frac{N \cdot s}{rad}\right]$	$b_{21}^*\left[\frac{N \cdot s}{rad \cdot kg}\right]$	R^2
1	0	0	1.121	0.022	14.251	0.289	0	0	0.5466
2	0	0	1.161	0.023	0	0	2.733	0.052	0.3639
3	4.356	0.084	0.432	0.008	9.894	0.183	0	0	0.5568
4	8.126	0.156	0.032	0.0005	0	0	0.805	0.014	0.4946

Table 1 Optimized damper coefficient values in each of the four configurations. Starred constants were normalized by the subject's body mass. Each value is an average across all optimized values found with 6 speeds and 5 subjects, for a total of 30 data points.

Case	t_{eng1} [%]	t_{dis1}[%]	t_{eng2}[%]	t_{dis2}[%]	θ_{eng1} [°]	θ_{dis1}[°]	θ_{eng2}[°]	θ_{dis2}[°]
1	51.3	64.7	86.0	95.1	15.5	52.8	35.8	9.8
2	51.3	64.1	86.0	92.3	15.5	49.6	36.0	13.2
3	51.3	64.2	86.1	95.2	15.5	49.7	36.9	10.3
4	51.3	63.8	85.7	95.2	15.5	49.0	39.0	10.3

Table 2 Optimized engagement/disengagement times for the two dampers in each of the four configurations. The engagement timing of the first damper was defined as the time at which knee torque crosses zero between 40% and 60% of the gait cycle with negative slope. Each value is the average across all optimized values found with 6 speeds and 5 subjects, for a total of 30 data points.

Despite the qualitative good fit, we obtain lower R^2 values than were found by Narang's work. Furthermore, while one of the major reasons for introducing a first-order component into the dampers is to smoothen the transition after the clutch engages and disengages, the predicted transitions are still quite sharp. This observation suggests that further work should consider engaging the damper exactly when the knee velocity is 0, as the damper torque is directly proportional to knee velocity.

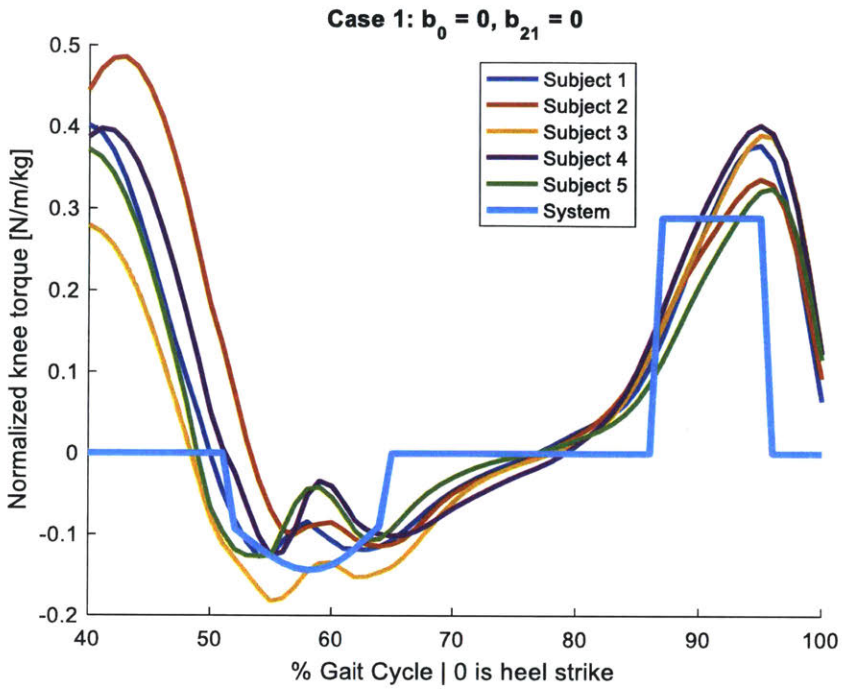

Figure 11 Normalized knee torque profile over the gait cycle segment with active dampers. Each subject's torque profile is the average profile from walking data collected at six different speeds. Torque profiles are normalized by dividing through by subject body mass. Inputs to the passive system are averaged position and velocity data. This plot shows the optimized result with a viscous damper for phase 2 and a friction damper for phase 3.

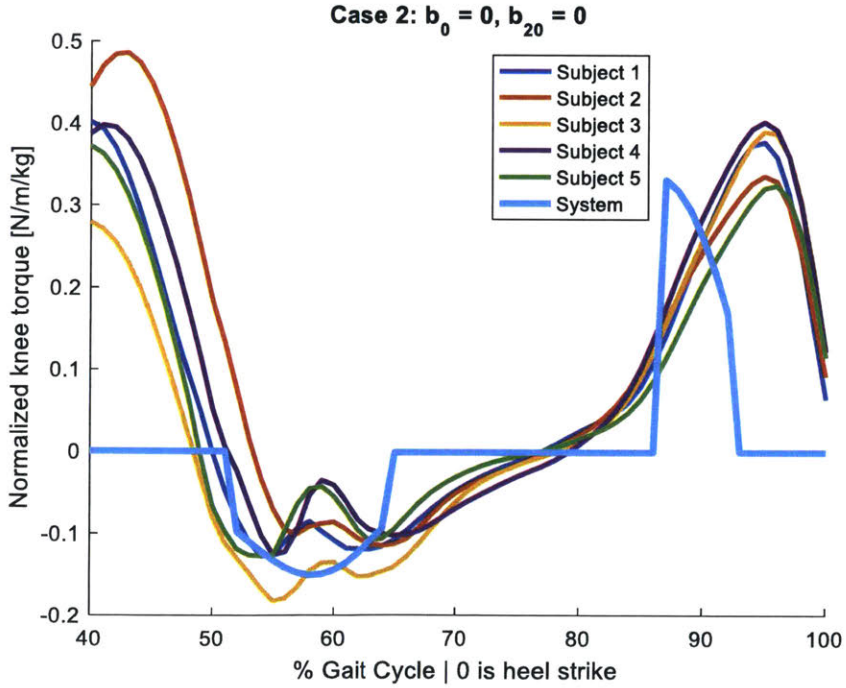

Figure 12 Normalized knee torque profile over the gait cycle segment with active dampers. Each subject's torque profile is the average profile from walking data collected at six different speeds. Torque profiles are normalized by dividing through by subject body mass. Inputs to the passive system are averaged position and velocity data. This plot shows the optimized result with a viscous damper for phases 2 and 3.

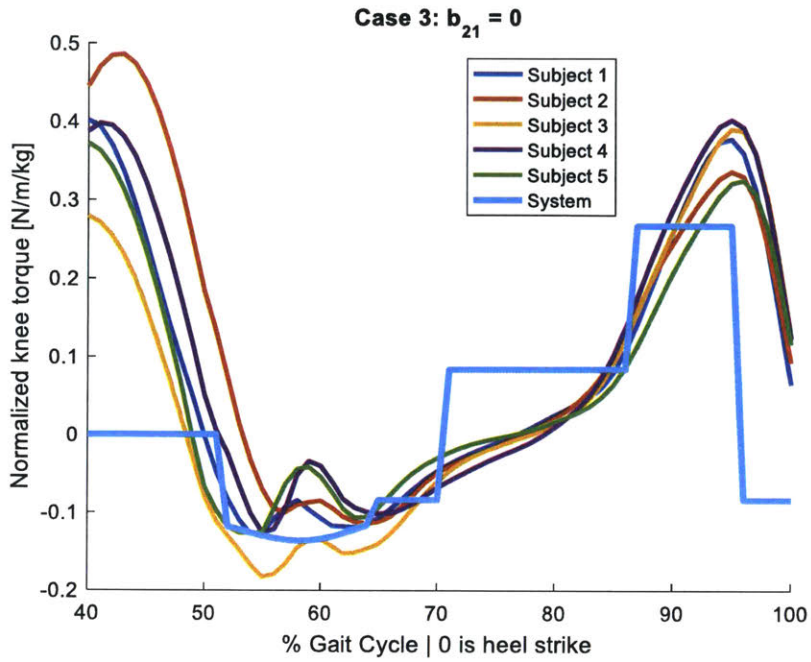

Figure 13 Normalized knee torque profile over the gait cycle segment with active dampers. Each subject's torque profile is the average profile from walking data collected at six different speeds. Torque profiles are normalized by dividing through by subject body mass. Inputs to the passive system are averaged position and velocity data. This plot shows the optimized result with a viscous damper for phase 2, a friction damper for phase 3, and a constant friction damper throughout phases 2 and 3.

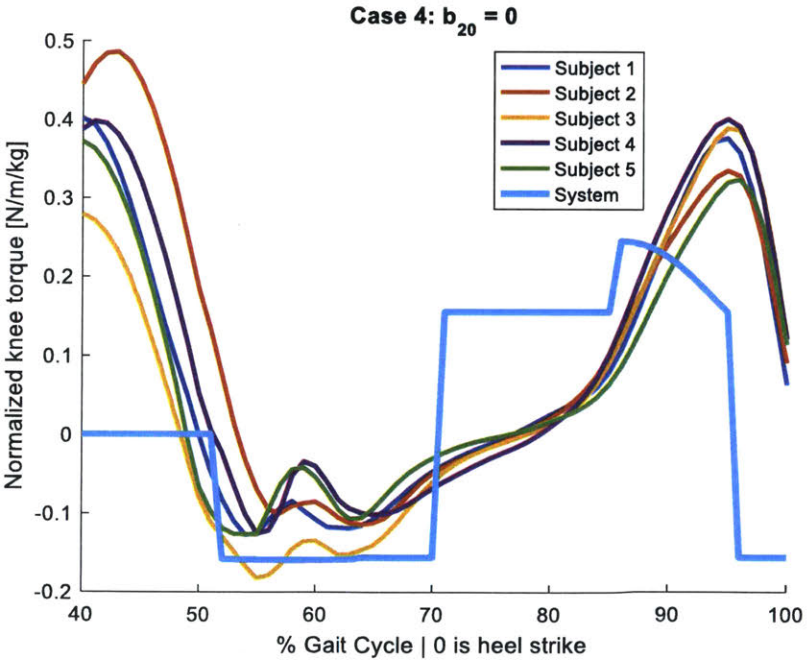

Figure 14 Normalized knee torque profile over the gait cycle segment with active dampers. Each subject's torque profile is the average profile from walking data collected at six different speeds. Torque profiles are normalized by dividing through by subject body mass. Inputs to the passive system are averaged position and velocity data. This plot shows the optimized result with a viscous damper each for phases 2 and 3, and an additional constant friction damper throughout both phases.

3.2 Effects of Cadence

The speed of walking can have significant effects on the torque profile seen at the knee during gait. In order to determine the relevance of walking speed for joint kinematics, we use the recently released Human Motion Dynamics open database from TU Darmstadt (Germany), which includes motion capture and EMG measurements for one male subject and one female subject walking. Figure 15 plots the averaged angular acceleration of the knee joint across the gait cycle for each walking speed. We see that the form of the curves are similar across the different cadences, but that the actual values vary significantly. From 1 to 2 m/s, there is approximately a 74% increase in the maximum angular acceleration.

Furthermore, amputees walk at a lower cadence than able-bodied individuals, and thus some of the differences in gait are a result of the lower speeds. We do not have cadence data available, so we use walking speed as a variable that roughly correlates with cadence. The average optimized parameters at 0.75 m/s are listed in Tables 3 and 4 below. Figures 16 to 19 plot the optimized profile for each case against the data for each subject walking at 0.75 m/s.

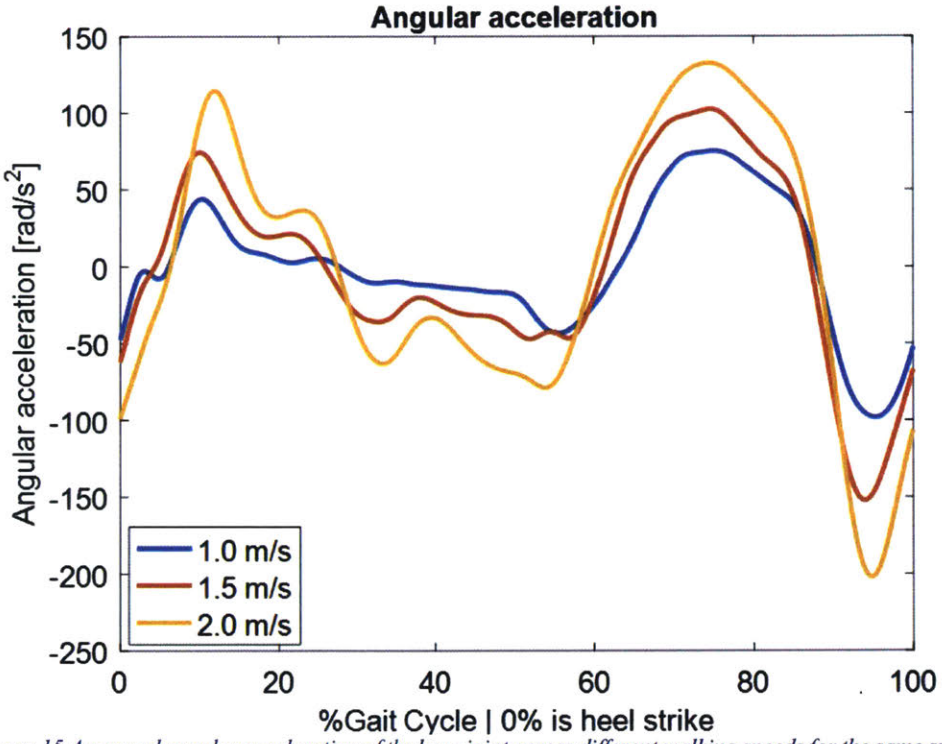

Figure 15 Averaged angular acceleration of the knee joint across different walking speeds for the same subject.

Case	$b_0\left[\frac{N}{rad}\right]$	$b_0^*\left[\frac{N}{rad \cdot kg}\right]$	$b_{11}\left[\frac{N \cdot s}{rad}\right]$	$b_{11}^*\left[\frac{N \cdot s}{rad \cdot kg}\right]$	$b_{20}\left[\frac{N}{rad}\right]$	$b_{20}^*\left[\frac{N}{rad \cdot kg}\right]$	$b_{21}\left[\frac{N \cdot s}{rad}\right]$	$b_{21}^*\left[\frac{N \cdot s}{rad \cdot kg}\right]$	R^2
1	0	0	1.268	0.017	8.217	0.117	0	0	0.5901
2	0	0	1.317	0.018	0	0	1.690	0.024	0.5978
3	1.981	0.028	0.885	0.012	6.233	0.088	0	0	0.5389
4	6.379	0.090	0.112	0.002	0	0	0.100	0.001	0.5174

Table 3 Optimized damper coefficient values in each of the four configurations at 0.75 m/s walking speed. Starred constants have been normalized by the subject's body mass. Each value is an average across all optimized values found with 5 subjects.

Case	t_{eng1}	t_{dis1}	t_{eng2}	t_{dis2}	$\theta_{eng1}[°]$	$\theta_{dis1}[°]$	$\theta_{eng2}[°]$	$\theta_{dis2}[°]$
1	54	65.3	83.3	95.7	17.1	45.8	41.5	7.6
2	54	63.5	80.3	95.7	17.1	39.8	49.6	8.4
3	54	61.5	83.3	95.8	17.1	33.5	33.5	8.4
4	54	63.8	81.5	95.9	17.1	34.1	34.1	8.4

Table 4 Optimized engagement/disengagement times for the two dampers in each of the four configurations at a walking speed of 0.75 m/s. The engagement timing of the first damper was defined as the time at which knee torque crosses zero between 40% and 60% of the gait cycle with negative slope. Each value is the average across all optimized values found with 5 subjects.

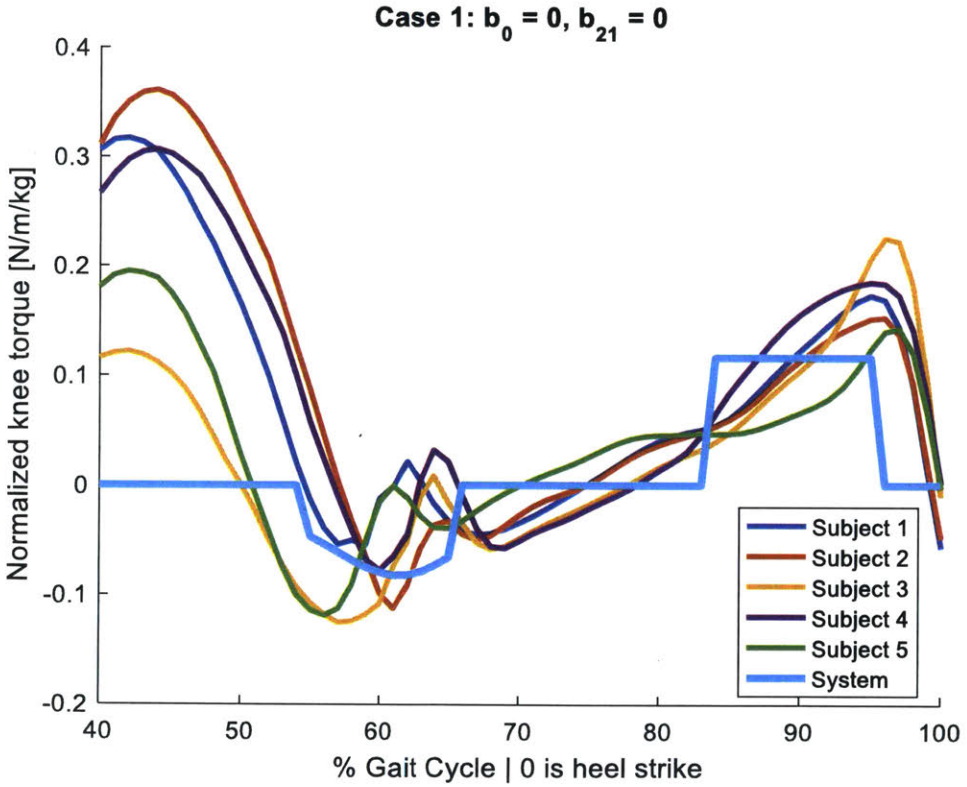

Figure 16 Normalized knee torque profile over the gait cycle segment with active dampers for a walking speed of 0.75 m/s. Torque profiles are normalized by dividing through by subject body mass. Inputs to the passive system are averaged position and velocity data from all the subjects walking at 0.75 m/s. This plot shows the optimized result with a viscous damper for phase 2 and a friction damper for phase 3.

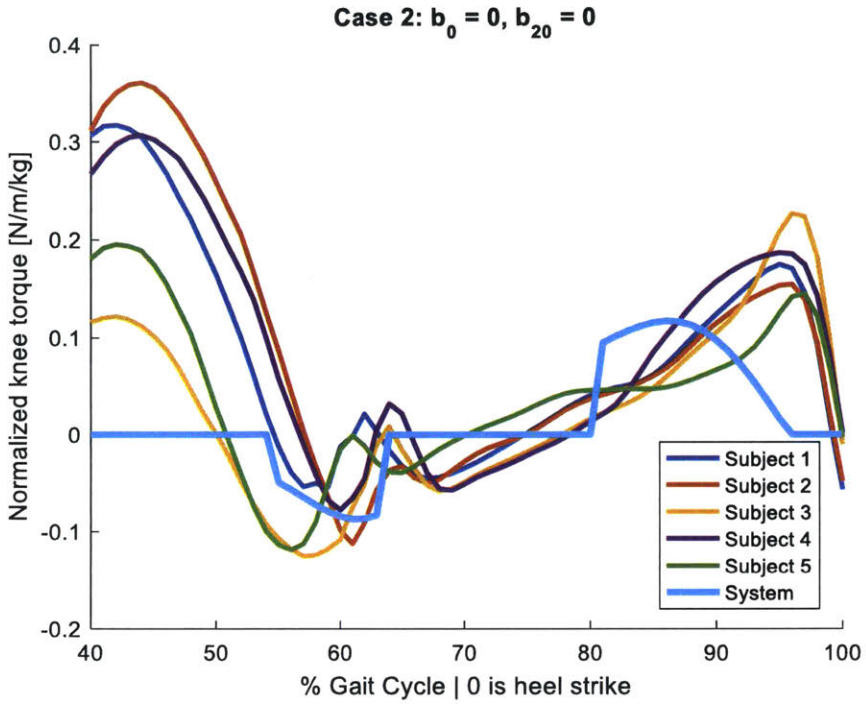

Figure 17 Normalized knee torque profile over 40%-100% of the gait cycle at 0.75 m/s. Torque profiles are normalized by dividing by subject body mass. Inputs to the passive system are averaged position and velocity data from all the subjects at 0.75 m/s. Plot shows the optimized result with a viscous damper for both phases.

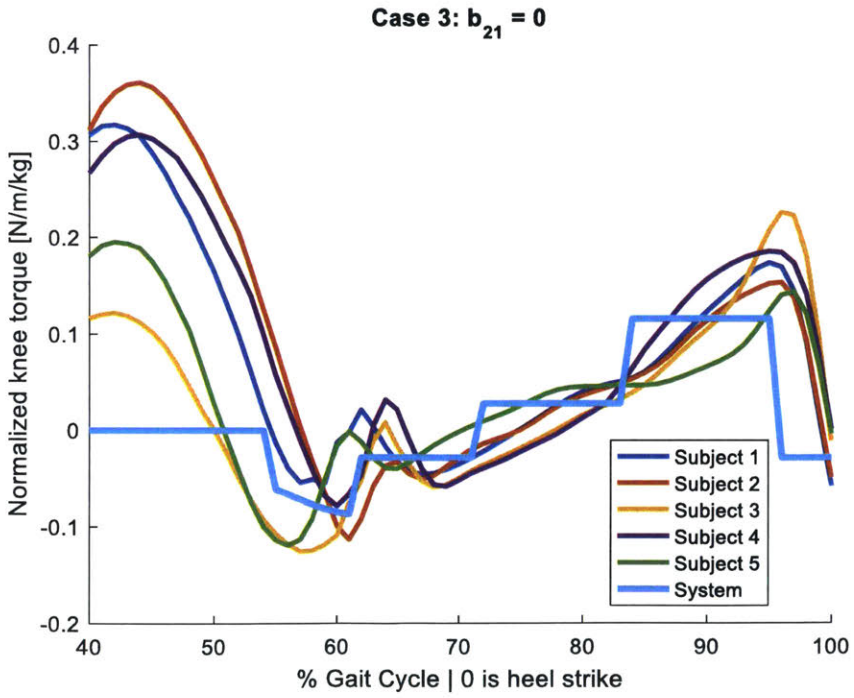

Figure 18 Normalized knee torque profile over 40%-100% of the gait cycle at 0.75 m/s. Torque profiles are normalized by dividing through by subject body mass. Inputs to the passive system are averaged position and velocity data from all the subjects walking at 0.75 m/s. This plot shows the optimized result with a viscous damper for phase 2, a friction damper for phase 3, and a constant friction damper throughout phases 2 and 3.

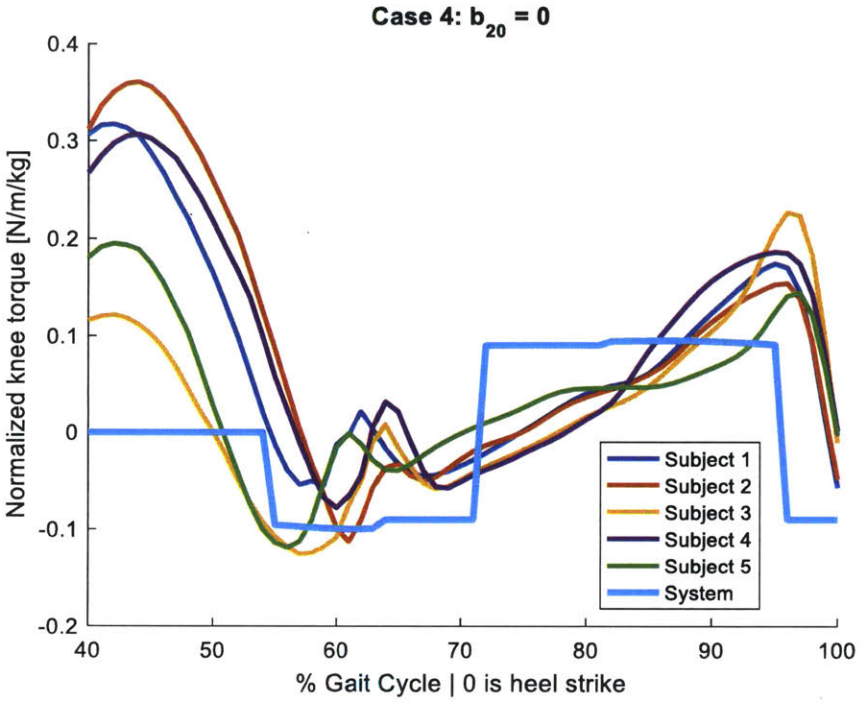

Figure 19 Normalized knee torque profile over 40%-100% of the gait cycle at 0.75 m/s. Torque profiles are normalized by dividing through by subject body mass. Inputs to the passive system are averaged position and velocity data from all the subjects walking at 0.75 m/s. This plot shows the optimized result with a viscous damper each for phases 2 and 3, and an additional constant friction damper throughout both phases.

We see that there is a sizeable difference between the mean profiles and optimized parameters in Figures 11 through 14 and Tables 1 and 2 in comparison with the profiles and parameters for a single speed, seen in Figures 16 through 19 and Tables 3 and 4. We plot the progression of the average of each optimized coefficient across the different speeds in Figures 20 through 23 for Subject 1 alone. These trends are seen in other subjects as well.

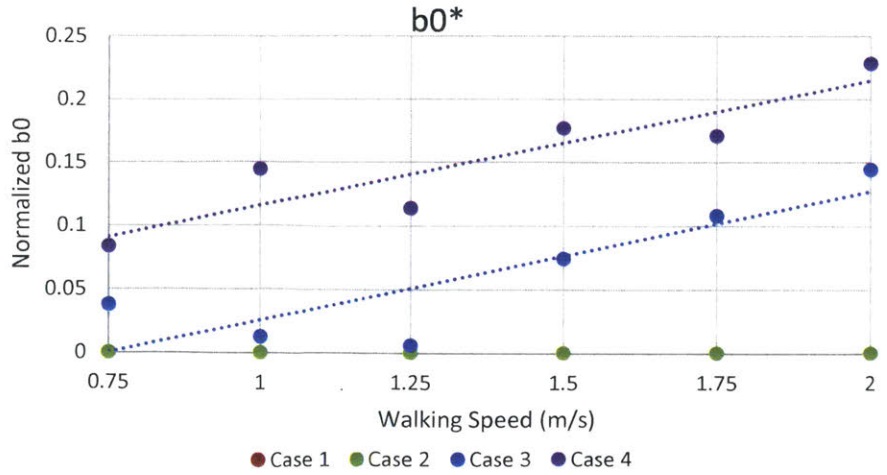

Figure 20 Optimized and normalized values for b_0 at each walking speed for Subject 1. The slope of the linear regression line for Case 3 is 0.101 and for Case 4 is 0.099. This implies that b_0 is dependent on walking speed.

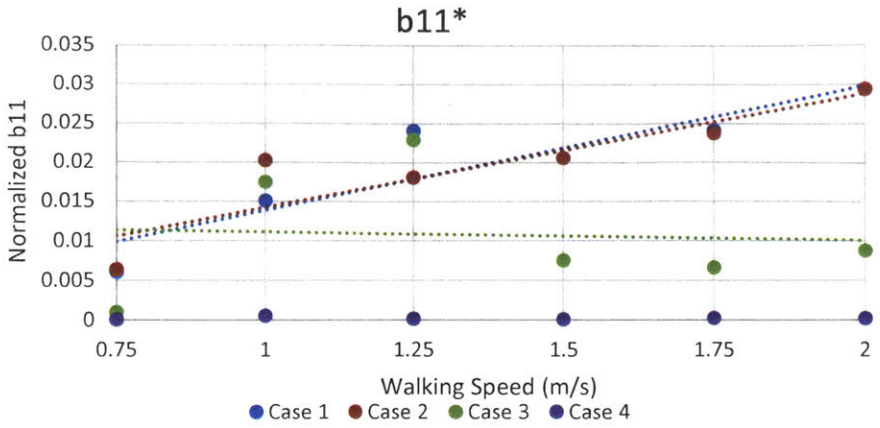

Figure 21 Optimized and normalized values for b_{11} at each speed for Subject 1. The slope of the linear regression line for Case 1 is 0.016, for Case 2 is 0.0146, and for Case 3 is -0.001. b_{11} varies with walking speed without constant friction damping.

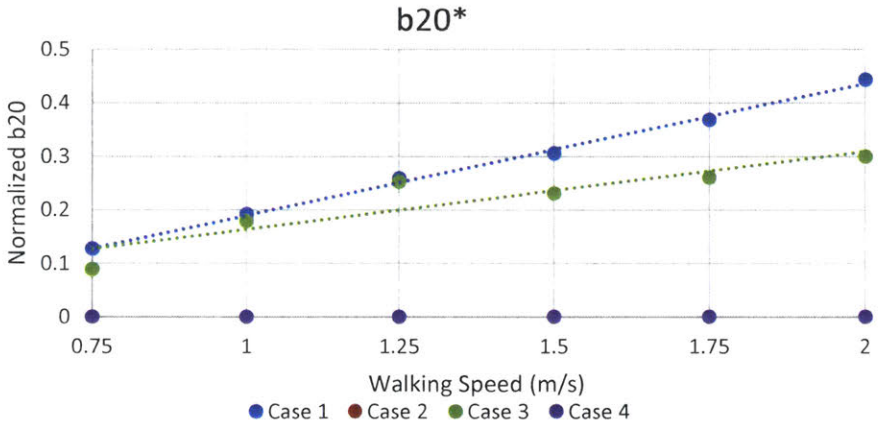

Figure 22 Optimized and normalized values for b_{20} at each walking speed for Subject 1. The slope of the linear regression line for Case 1 is 0.246 and for Case 3 is 0.145. Thus, b_{20} is also dependent on walking speed.

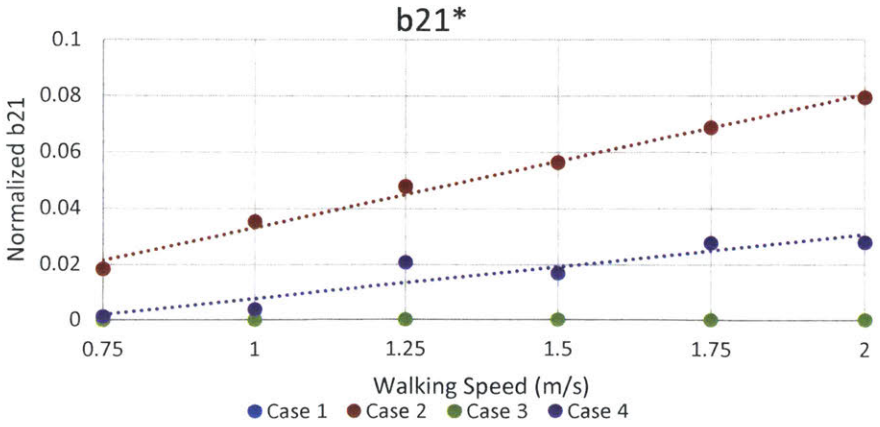

Figure 23 Optimized and normalized values for b_{21} at each walking speed for Subject 1. The slope of the linear regression line for Case 2 is 0.047 and for Case 2 is 0.023. This implies that b_{21} is dependent on walking speed.

3.3 Effects of Mass

We know that varying masses leads to a difference in generated torques. Varying the masses from 25% to 100% of the able-bodied masses and plotting the torques at the knee joint, as calculated by the inverse dynamics model, we obtain the result seen in Figure 23. We see that at the knee, there is a maximum difference of 75% between the 50% and 100% mass cases. Thus, we cannot ignore mass differences between amputee and able-bodied limbs when conducting further analysis.

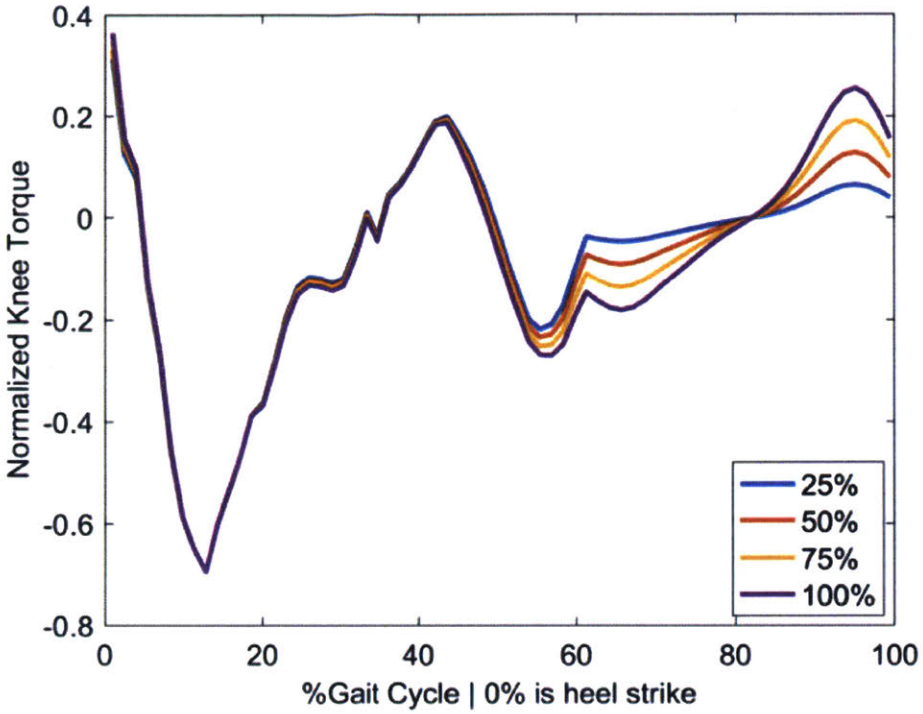

Figure 24 Torque profile generated at the knee under varying leg segment masses. Our inverse dynamics model was used to generate these plots. There are significant differences between the incremental cases during the swing phase.

To observe the effects of mass on our optimization, we plot the averaged optimized parameters for each case as a function of subject body mass. The subjects in the study were chosen within a given mass range in order to reduce variability, so any differences that we see are likely to be minimal. Figures 25 through 28 contain plots analogous to Figures 20-23, but with parameters varying across the subjects' body masses. We must also be mindful of the existing natural variation between individuals. Based on the curves presented here, we are justified in using body mass-normalized parameters, but focusing on the effects of velocity on optimization.

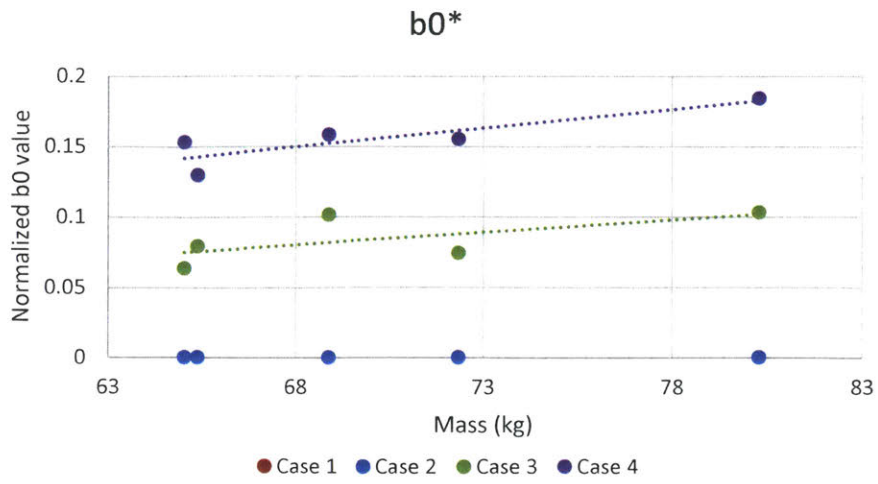

Figure 25 Optimized and normalized values for b_0 for each represented body mass averaged across all walking speeds. The slope of the linear regression line for Case 3 is 0.003 and for Case 4 is 0.002. These values are two orders of magnitude smaller than the slopes of b_0 vs walking speed, and thus, we conclude that body mass does not greatly affect the optimization of b_0.

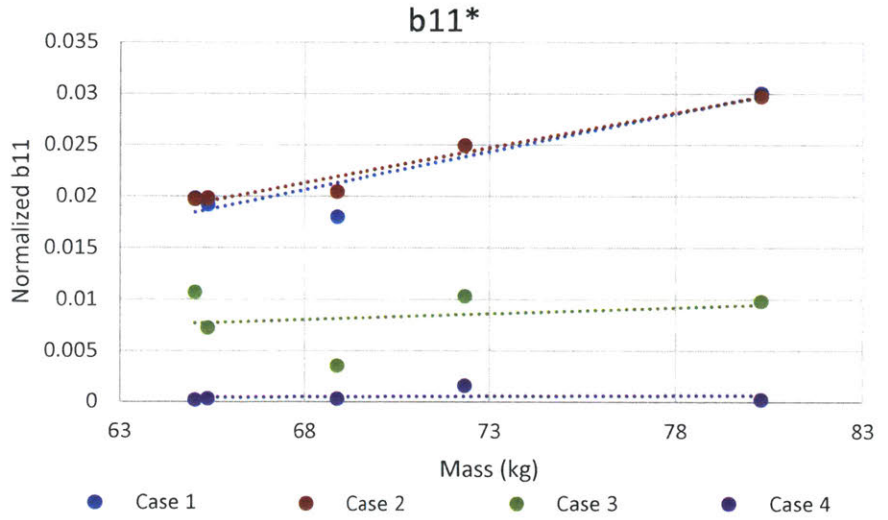

Figure 26 Optimized and normalized values for b_0 for each represented body mass averaged across all walking speeds. The slope of the linear regression line for Case 1 is 0.0007, for Case 2 is 0.0007, and for Case 3 is 0.0001. These values are two orders of magnitude smaller than the slopes of b_{11} vs walking speed, and thus, we conclude that body mass does not greatly affect the optimization of b_{11}.

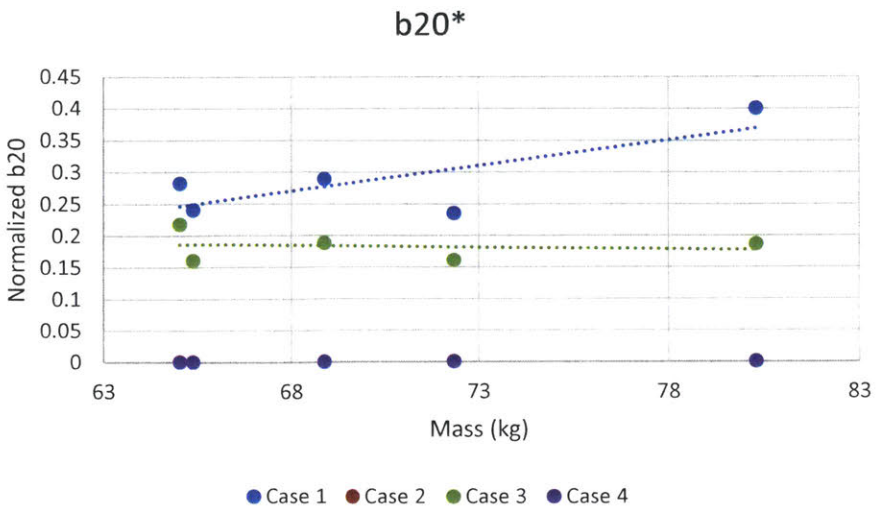

Figure 27 Optimized and normalized values for b_0 for each represented body mass averaged across all walking speeds. The slope of the linear regression line for Case 1 is 0.008 and for Case 3 is -0.0006. These values are two orders of magnitude smaller than the slopes of b_{20} vs walking speed, and thus, we conclude that body mass does not greatly affect the optimization of b_{20}.

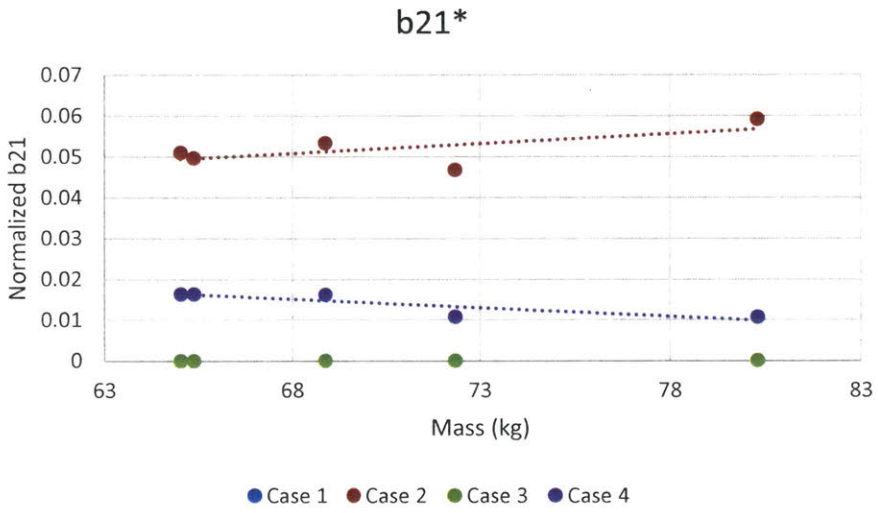

Figure 28 Optimized and normalized values for b_0 for each represented body mass averaged across all walking speeds. The slope of the linear regression line for Case 2 is 0.005 and for Case 4 is -0.0004. These values are two orders of magnitude smaller than the slope of b_{21} vs walking speed, and thus, we conclude that body mass does not greatly affect the optimization of b_{21}.

4. Discussion and Conclusions

The results of this study build on prior work done in the MIT GEAR Lab, and enables the continuation of analysis with the framework set up through these algorithms. Through this work, we have developed an accessible optimization algorithm that can be iterated upon further to continue the investigation. We have successfully applied this algorithm to a recent open-source dataset published by the MIT Biomechatronics Group. After running the 120 simulations, we find

that the best fit, as measured by the highest R^2 value, is obtained in configuration 3, in which a viscous damper is active during phase 2, a friction damper is active during phase 3, and an additional friction damper is active from phase 2 till the end of the gait cycle. We make the suggestion that $b_0^* = 0.084, b_{11}^* = 0.008, b_{20}^* = 0.183$, gives the most optimal passive system knee torque with the engagement and disengagement timings $t_{eng1} = 51.3\%, t_{dis1} = 64.2\%, t_{eng2} = 86.1\%, t_{dis2} = 95.2\%$.

We then proceeded to study the relationship between the optimized values and walking speed. The study concludes that all four optimized and normalized parameters display positive correlation with walking speed. This suggests that further understanding of the cadence of amputees will be required to effectively optimize the system.

Finally, we explored the effects of body mass on the optimized parameter values. We find that there is a positive correlation here as well. However, the slopes of the linear regression fit lines approximately two orders smaller in magnitude than those relating parameters and walking speed. Thus, the influence of body mass is negligible in comparison to the influence of cadence.

The successful development of an effective passive prosthetic knee joint opens up a plethora of potential new applications. The same methods may be applied to other joints such as the hip or ankle, both of which also play crucial roles in defining gait [5]. Moreover, the benefits of the device being low-cost and affordable would allow for a number of amputees to be able to regain mobility and thus, regain their self-sufficiency. In many developing countries where physical labor is a major component of an individual's livelihood, affordable and effective prostheses can help revive economies from the level of the individual, and return dignity to amputees who may have been unemployed previously.

At a larger scale, an expanded mobilized work force strengthens economies and builds up labor infrastructures. Such changes have the potential to lead to a positive feedback loop in which increased labor infrastructure increases national revenues, which enables larger investment in healthcare, further increasing the labor force. Moreover, higher quality healthcare improves national image, further spurring economic growth [14]. Thus, it is crucial for us to work towards enabling self-sufficiency for all individuals irrespective of physical ability.

There are a few limitations to the methods and findings presented here that are important to be cognizant of. The Biomechatronics dataset that we are using in this study is a significant improvement from prior work as we are able to use data from one source to complete all of the analysis, thereby ensuring that differences between experimental setups do not affect our results. However, the participants in the study were barefoot during measurements, which may affect the the center of pressure data depending on the subject's foot architecture. This information is used by SIMM to determine the appropriate torques, and hence, torque errors may be propagated. However, from Figure 11, these differences are likely insignificant as the torque profiles from the Winter dataset aligns well with those from Biomech. The data is also only collected from males within a given age and weight range. So additional studies are needed to study the variations between genders, age groups, and body masses.

In our model, we also consider the effects of inactive dampers and clutches as insignificant. However, further study will be required to determine whether there are nonlinearity effects that are

important to include. Moreover, we find that the optimization protocol returns different values at times, and it would be interesting understand whether the walking speed itself is leading to this phenomenon or if there are additional factors to consider. In order to so, it is also important to redefine the cost function to more accurately reflect the waveform fit in addition to actual values.

Additionally, despite our goal of smoothening the transitions after the clutch engages and disengages with the new configuration, the predicted transitions are still abrupt due to the non-zero knee velocity at the time of each change. This observation suggests that further work should consider engaging the damper when knee velocity is 0 rather than when the knee torque is at 0.

We show in this thesis that body mass does not affect optimized parameters significantly. However, in addition to overall body weight, the distribution of weight may vary significantly between able-bodied individuals and amputees. Differences in individual segment masses, such as the shank or upper leg, may also lead to significantly different system behavior. Thus, further work in this area is required to understand the implications of varying masses for amputee gait.

In future research, it would be interesting to delve more into hip dynamics. Given our current model setup, the hip only provides reaction dynamics in the degrees of freedom that we are working with at the knee. However, the hip is a much more complicated joint, and likely provides additional reaction forces and torques as well. Looking into this structure in more detail could lead to insights for further work.

Finally, we can consider the case of bringing this concept back to higher-cost markets to provide a more affordable alternative to existing solutions. In these environments, it is feasible to incorporate an active component, such as a motor, that engages intermittently depending on the gait cycle timing. Further analysis of the normalized power profiles that were used previously to determine engagement and disengagement of the clutches could be used to inform where in the gait cycle to activate the motor for optimal performance. In this way, disruptive engineering used to innovate for low-cost environments could benefit users worldwide.

5. Appendices

Appendix A: Optimization Code

A.1 Optimization script

```
%% This script finds the optimal value for both dampers coefficients
clear all;
close all;
clc;

% Load subject data
M = load('Biomech Data/BC011113/walk150.mat');
% M = load('Biomech Data/DC011413/walk100.mat');
% M = load('Biomech Data/DH121412/walk200.mat');
% M = load('Biomech Data/JB011613/walk200.mat');
% M = load('Biomech Data/MC121812/walk200.mat');
% M1 = xlsread('Winter_Appendix_data.xlsx','A4.RelJointAngularKinematics');
%
% % Time
```

```
% t = M1(29:96,2);
% t = linspace(0,100,length(t))';
% % Angle position, velocity, and acceleration
% th_k = M1(29:96,6)*pi/180;
% w_k = M1(29:96,7);

% M2 = xlsread('Winter_Appendix_data.xlsx','A5.ReactionForces&Moments');
% T_k_data = -M2(29:96,15); %definition in dataset opposite to ours

% global passives damps1 damps2 costs
% passives = [];
% damps1 = [];
% damps2 = [];
% costs = [];
%% Data

A = M;
% Time
t = [0:100];

mass = A.mass; %Full body mass in kg
% mass = 56.29;

% Knee position and velocity
th_k = A.m_knee_ang_l*pi/180;
w_k = A.m_knee_vel_l;

% Knee torque
T_k_data = A.m_knee_mom_l;

% Power
% P_k = T_k_data.*w_k;

teng1 = (find((abs(T_k_data))<3));
ind = (teng1>40 & teng1<60);
teng1 = teng1(ind);
teng1 = teng1(1);
thpk = find(th_k == max(th_k));
t_thpk = t(thpk);

%% Different configurations
%x = [tdis1 b0 b11 teng2 tdis2 b20 b21]

% Case 1: b0 = 0, b21 = 0 (damper 2 is friction)
Aeq = [];
beq = [];
% lb = [teng1+5,0,0,t_thpk,t_thpk+3,0,0];
% ub = [t_thpk,0,150,100,100,150,0];

% % Case 2: b0 = 0, b20 = 0 (damper 2 is viscous)
% lb = [teng1+5,0,0,t_thpk,t_thpk+3,0,0];
% ub = [t_thpk,0,150,100,100,0,150];

% % Case 3: b21 = 0 (const friction damper + damper 2 is friction)
% lb = [teng1+5,0,0,t_thpk,t_thpk+3,0,0];
% ub = [t_thpk,150,150,100,100,150,0];
```

```
% % Case 4: b20 = 0 (constant friction damper + damper 2 is viscous)
lb = [teng1+5,0,0,t_thpk,t_thpk+3,0,0];
ub = [t_thpk,150,150,100,100,0,150];

A = [0 0 0 1 -1 0 0];
b = [-3];
nonlcon = [];
[x,fval,exitflag,output]                                                    =
ga(@(x)costf_dampers(M,x),7,A,b,Aeq,beq,lb,ub,nonlcon)
tdis1 = x(1);
b0 = x(2);
b11 = x(3);
teng2 = x(4);
tdis2 = x(5);
b20 = x(6);
b21 = x(7);

%% Dissipative Phases
T_const = (t>teng1).*(-sign(w_k).*b0);
T_damp1 = (t>teng1 & t<tdis1).*(-b11.*w_k);
T_damp2 = (t>teng2 & t<tdis2).*(-sign(w_k).*b20-b21.*w_k);
T_passive = (t>teng1).*(T_damp1+T_damp2+T_const);
plot(t,T_passive,t,T_k_data);
legend('Model','Data');

th_eng1 = th_k(floor(teng1))*180/pi;
th_eng2 = th_k(floor(teng2))*180/pi;
th_dis1 = th_k(floor(tdis1))*180/pi;
th_dis2 = th_k(floor(tdis2))*180/pi;
```

A.2 Cost function

```
function [cost_dampers] = costf_dampers(A,x)

% global passives damps1 damps2 costs
% Time
t = [0:100];

% Knee position and velocity
th_k = A.m_knee_ang_l*pi/180;
w_k = A.m_knee_vel_l;

% Knee torque
T_k_data = A.m_knee_mom_l;

%% Parameters
mass = A.mass; %Full body mass in kg

%% Dissipative Phases
teng1 = (find((abs(T_k_data))<3));
ind = (teng1>40 & teng1<60);
teng1 = teng1(ind);
teng1 = teng1(1);
T_damp1 = (t>=teng1 & t<=(x(1))).*(-sign(w_k)*x(2)-x(3)*w_k);
T_damp2 = (t>=(x(4)) & t<=(x(5))).*(-sign(w_k).*(x(2)+x(6))-x(7).*w_k);
T_passive = (t>teng1).*(T_damp1+T_damp2);
```

```
teng1 = find(t == floor(teng1));
teng1 = teng1(1);
[r2 rsme] = rsquare(T_k_data(teng1:end), T_passive(floor(teng1):end),true);
cost_dampers = 1-r2;
end
```

A.3 RSquare function

```
function [r2 rmse] = rsquare(y,f,varargin)
% Compute coefficient of determination of data fit model and RMSE
%
% [r2 rmse] = rsquare(y,f)
% [r2 rmse] = rsquare(y,f,c)
%
% RSQUARE computes the coefficient of determination (R-square) value from
% actual data Y and model data F. The code uses a general version of
% R-square, based on comparing the variability of the estimation errors
% with the variability of the original values. RSQUARE also outputs the
% root mean squared error (RMSE) for the user's convenience.
%
% Note: RSQUARE ignores comparisons involving NaN values.
%
% INPUTS
%   Y       : Actual data
%   F       : Model fit
%
% OPTION
%   C       : Constant term in model
%             R-square may be a questionable measure of fit when no
%             constant term is included in the model.
%   [DEFAULT] TRUE : Use traditional R-square computation
%             FALSE : Uses alternate R-square computation for model
%                     without constant term [R2 = 1 - NORM(Y-F)/NORM(Y)]
%
% OUTPUT
%   R2      : Coefficient of determination
%   RMSE    : Root mean squared error
%
% EXAMPLE
%   x = 0:0.1:10;
%   y = 2.*x + 1 + randn(size(x));
%   p = polyfit(x,y,1);
%   f = polyval(p,x);
%   [r2 rmse] = rsquare(y,f);
%   figure; plot(x,y,'b-');
%   hold on; plot(x,f,'r-');
%   title(strcat(['R2 = ' num2str(r2) '; RMSE = ' num2str(rmse)]))
%
% Jered R Wells
% 11/17/11
% jered [dot] wells [at] duke [dot] edu
%
% v1.2 (02/14/2012)
%
% Thanks to John D'Errico for useful comments and insight which has helped
% to improve this code. His code POLYFITN was consulted in the inclusion of
```

```
% the C-option (REF. File ID: #34765).

if isempty(varargin); c = true;
elseif length(varargin)>1; error 'Too many input arguments';
elseif ~islogical(varargin{1}); error 'C must be logical (TRUE||FALSE)'
else c = varargin{1};
end

% Compare inputs
if ~all(size(y)==size(f)); error 'Y and F must be the same size'; end

% Check for NaN
tmp = ~or(isnan(y),isnan(f));
y = y(tmp);
f = f(tmp);

if c; r2 = max(0,1 - sum((y(:)-f(:)).^2)/sum((y(:)-mean(y(:))).^2));
else r2 = 1 - sum((y(:)-f(:)).^2)/sum((y(:)).^2);
    if r2<0
    % http://web.maths.unsw.edu.au/~adelle/Garvan/Assays/GoodnessOfFit.html
        warning('Consider adding a constant term to your model') %#ok<WNTAG>
        r2 = 0;
    end
end

rmse = sqrt(mean((y(:) - f(:)).^2));
```

6. References

[1] "Prosthetics in Resource-Limited Countries | June 2015 | The O&P EDGE | oandp.com." [Online]. Available: http://www.oandp.com/articles/2015-06_02.asp. [Accessed: 24-Oct-2016].

[2] "Prosthetics in the developing world: a review of the literature | O&P Virtual Library." [Online]. Available: http://www.oandplibrary.org/poi/1996_01_051.asp. [Accessed: 24-Oct-2016].

[3] R. A. Donatelli, "Abnormal biomechanics of the foot and ankle," *J. Orthop. Sports Phys. Ther.*, vol. 9, no. 1, pp. 11–16, 1987.

[4] F. Tian, M. S. Hefzy, and M. Elahinia, "A Biologically Inspired Knee Actuator for a KAFO," *J. Med. Devices*, vol. 10, no. 4, pp. 045001–045001, Aug. 2016.

[5] J. B. dec M. Saunders, V. T. Inman, and H. D. Eberhart, "The Major Determinants in Normal and Pathological Gait," *J Bone Jt. Surg Am*, vol. 35, no. 3, pp. 543–558, Jul. 1953.

[6] "Jaipur Foot | Stanford-Jaipur Knee | Jaipur Knee." [Online]. Available: http://jaipurfoot.org/what_we_do/prosthesis/stanford_jaipur_knee.html. [Accessed: 12-Dec-2016].

[7] V. N. M. Arelekatti and V. Winter Amos G., "Design of Mechanism and Preliminary Field Validation of Low-Cost, Passive Prosthetic Knee for Users With Transfemoral Amputation in India," p. V05AT08A043, Aug. 2015.

[8] Boundless, "Body Planes and Sections," *Boundless*, Dec. 2016.

[9] Y. S. Narang, V. N. M. Arelekatti, and A. G. Winter, "The Effects of Prosthesis Inertial Properties on Prosthetic Knee Moment and Hip Energetics Required to Achieve Able-

Bodied Kinematics," *IEEE Trans. Neural Syst. Rehabil. Eng.*, vol. 24, no. 7, pp. 754–763, Jul. 2016.
[10] D. A. Winter, *Biomechanics and Motor Control of Human Movement*. Wiley, 1990.
[11] Y. S. (Yashraj S. Narang, "Identification of design requirements for a high-performance, low-cost, passive prosthetic knee through user analysis and dynamic simulation," Thesis, Massachusetts Institute of Technology, 2013.
[12] V. N. M. Arelekatti and A. G. Winter, "Design of a fully passive prosthetic knee mechanism for transfemoral amputees in India," in *2015 IEEE International Conference on Rehabilitation Robotics (ICORR)*, 2015, pp. 350–356.
[13] J. Markowitz and H. Herr, "Human Leg Model Predicts Muscle Forces, States, and Energetics during Walking," *PLOS Comput. Biol.*, vol. 12, no. 5, p. e1004912, May 2016.
[14] C. Wendland, *A Heart for the Work.*.
[15] "Knee kinematics during gait." [Online]. Available: http://coph.ouhsc.edu/dthompso/web/pk/kneegraf.htm. [Accessed: 24-Oct-2016].
[16] P. M. Matters, "Abnormal gait." [Online]. Available: http://www.pmmonline.org/page.aspx?id=750. [Accessed: 18-May-2017].
[17] D. A. Winter and S. E. Sienko, "Biomechanics of below-knee amputee gait," *J. Biomech.*, vol. 21, no. 5, pp. 361–367, Jan. 1988.
[18] "BELOW-KNEE AMPUTEE RUNNING GAIT. : American Journal of Physical Medicine & Rehabilitation," *LWW*. [Online]. Available: http://journals.lww.com/ajpmr/Fulltext/1982/04000/BELOW_KNEE_AMPUTEE_RUNNING_GAIT_.2.aspx. [Accessed: 18-May-2017].
[19] R. Gailey, K. Allen, J. Castles, J. Kucharik, and M. Roeder, "Review of secondary physical conditions associated with lower-limb amputation and long-term prosthesis use," *J. Rehabil. Res. Dev.*, vol. 45, no. 1, pp. 15–29, Jan. 2008.
[20] "Muscle Power Compensatory Mechanisms in Below-Knee Amputee G... : American Journal of Physical Medicine & Rehabilitation," *LWW*. [Online]. Available: http://journals.lww.com/ajpmr/Fulltext/2001/01000/Muscle_Power_Compensatory_Mechanisms_in_Below_Knee.7.aspx. [Accessed: 18-May-2017].
[21] R. E. Seroussi, A. Gitter, J. M. Czerniecki, and K. Weaver, "Mechanical work adaptations of above-knee amputee ambulation," *Arch. Phys. Med. Rehabil.*, vol. 77, no. 11, pp. 1209–1214, Nov. 1996.